# Parameters of the 9.17 MeV level in $^{14}$N

W. Biesiot and Ph.B. Smith
*Laboratorium voor Algemene Natuurkunde, University of Gronigen, Gronigen, The Netherlands*
(Received 9 December 1980)

Mutually consistent measurements of elastic proton scattering and resonance absorption show that the width of the 9.17 MeV level in $^{14}$N ($\Gamma = 135 \pm 8$ eV) is almost twice as large as the accepted literature value. The positive parity is unambiguously confirmed. The excitation energy is determined to be $9172.5 \pm 0.3$ keV, based upon a cascade-crossover technique with a $^{56}$Co source for calibration. The expected azimuthal asymmetry of the resonance fluorescence of the plane-polarized photons at this resonance is demonstrated quantitatively.

[NUCLEAR REACTIONS $^{13}$C$(p,\gamma)^{14}$N, $^{13}$C $(p,p)^{13}$C, $^{14}$N res. abs., $^{14}$N res. fluor., $E = 1.75$ MeV; measured $\sigma(E,E_p,\theta)$. $^{14}$N deduced levels $J$, $\pi$, $\Gamma$, levels. Enriched target.]

## I. INTRODUCTION

One of the strongest known $(p,\gamma)$ resonances is the $E_p = 1.75$ MeV resonance in the $^{13}$C$(p,\gamma)^{14}$N reaction, leading to the 9.17 MeV level in $^{14}$N. Spectroscopic information regarding this level and its decay has recently been summarized.[1] In order to establish more accurate and reliable results for several parameters, we have applied an array of experimental techniques. In Sec. II an elastic proton scattering experiment is described, which results unambiguously in a parity determination as well as in a new value of $\Gamma_p$. The excitation energy was obtained accurately by comparing the lines occurring in the cascades via the 5.69 and 6.45 MeV levels in $^{14}$N with the precisely known lines from a $^{56}$Co source (Sec. III). Resonance absorption experiments were performed to obtain values for $\Gamma$ and $\Gamma_{\gamma_0}$. Some general features of the method are discussed. This work is contained in Sec. IV. Section V is devoted to the description and interpretation of measurements with a new variant of the nuclear resonance fluorescence technique, with the monoenergetic polarized photons emitted at this resonance. In the last section the results of the different methods are discussed and compared.

## II. PROTON ELASTIC SCATTERING EXPERIMENTS

The proton yield as a function of incoming beam energy was measured in the vicinity of the $E_p = 1.75$ MeV resonance in the $^{13}$C$(p,p)^{13}$C reaction. The effective energy of the incident protons was varied by changing a positive voltage applied to the target with respect to ground. A range of 3 keV was scanned in 25 steps. The scattered protons were detected at three angles (88°, 124°, and 174°) by thin, high-resolution, silicon detectors (typical value of the FWHM: 7 keV at 2 MeV). Two types of targets were used: a self-supporting 4 $\mu$g/cm$^2$ carbon foil (80% $^{13}$C) and a 1 $\mu$g/cm$^2$ thick $^{13}$C target deposited on a 10 $\mu$g/cm$^2$ Formvar backing. The beam current was about 50 nA.

A typical proton spectrum is shown in Fig. 1.

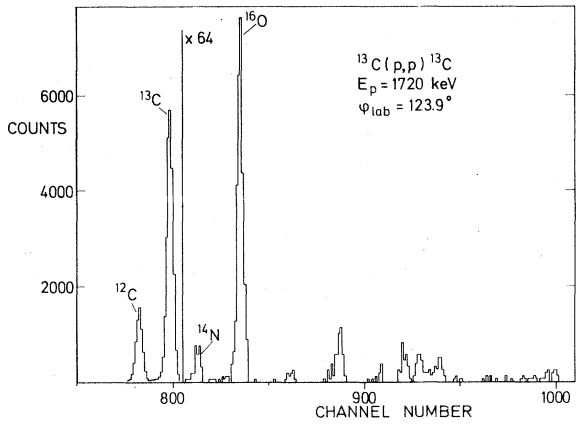


FIG. 1. Typical spectrum of protons elastic scattered at $E_p = 1.72$ MeV. The target is a 4 $\mu$g/cm$^2$ thick self-supporting carbon foil (80% $^{13}$C).

 

Determination of the $^{13}C$ line contents is not difficult due to the complete resolution of the $^{12}C$ and $^{13}C$ peaks. The resulting data points with associated standard deviations are shown in Fig. 2.

The same method of analysis was followed as in an earlier publication.[2] The $^{13}C$ nucleus has a ground-state spin of $\frac{1}{2}^-$, so the channel spin $S$ can have the values $0^-$ or $1^-$. The spin of the 9.17 MeV level has already been determined to be 2 by means of angular distribution and angular correlation studies.[3-5]

The off-resonance differential cross section $\sigma_p(\phi)$ is larger than the calculated Rutherford value $[\sigma_p^R(\phi)]$. The ratio $f$ between these quantities was determined by measuring the proton and alpha scattering yield at several energies in the vicinity of 1.75 MeV. The quantity $f$ is found from these measurements as

$$f=\frac{\sigma_p(\phi)}{\sigma_\alpha(\phi)}\frac{\sigma_\alpha^R(\phi)}{\sigma_p^R(\phi)}, \tag{1}$$

where $\sigma_\alpha$ is the experimental cross section in $\alpha$ scattering and $\sigma_\alpha^R$ is the calculated Rutherford cross section. The ratio $f$ was calculated from Eq. (1) on the assumption that the alpha scattering at 1.75 MeV is a pure Rutherford process. This assumption was confirmed by separate experiments. The values for $f$ were about 2.6 (at 88°), 5.1 (at 124°), and 6.8 (at 174°), the error being about 4%.

The computer code of Ref. 2 was used in order to obtain the relevant level parameters for both possible $J^\pi$ assumptions. In the fitting process the width of the gamma decay is taken to be $\Gamma_\gamma=7.7\pm0.9$ eV, based upon Ref. 1. The results are summarized in Table I and make clear that the $J^\pi=2^-$ assumption is excluded as the associated normalized $\chi^2$ does not fall below the value corresponding to the 0.1% confidence level for this fit. Moreover, the instrumental width as obtained for the $J^\pi=2^-$ case is nonphysical as it is 50% higher than the value that would follow from target thickness and spread in proton beam energy. A difficulty in the analysis was that in all cases the results of a fit to the 174° data were inconsistent with the values obtained by fits to the other angles, due to straggling effects not incorporated in the computer code. This is illustrated in Fig. 2, where the solid lines are calculated with parameters from a simultaneous fit to the 88° and 124° data. The fit at 174° is adequate, except in the tail, where the straggling effects are most serious, especially for the thicker of the two targets. A separate fit to the 174° data results in nonphysical values of the parameters. The parameter values obtained are not influenced by more than the error limits by variations in the ratio $f$ (see above) corresponding to the experimental error in this quantity. The propagation of this error and of the error in $\Gamma_\gamma$ was taken into account in the error stated for $\Gamma_p$. The dashed lines in Fig. 2 indicate the best fit after omitting the hard-sphere contribution to the interference terms.

The mean value for $\Gamma_p$ from both experiments is $127\pm8$ eV, which leads with $\Gamma_\gamma=8$ eV to a value for the total width of $135\pm8$ eV. The amplitude ratio for the $f$ and $p$ proton wave functions is calculated from our experiments to be $-0.73\pm0.06$, in agreement with the value of $-0.70\pm0.26$ found by Prosser *et al.*[3] The Huby[6] correction is applied here for the phase convention.

In a preliminary publication more than 20 years ago, Strassenburg *et al.*[7] reported the results of a determination of the polarization of the 9.17 MeV gamma rays from the $E_p=1.75$ MeV resonance in $^{13}C(p,\gamma)^{14}N$. They concluded that their results were consistent with $1^+$ or $2^+$. As the $J=1$ possibility is excluded by the angular distribution measurements described above, a $2^+$ assignment remains. The results of our study confirm unambiguously the positive parity assignment to the 9.17 MeV $^{14}N$ level.

## III. EXCITATION ENERGIES

With the accurately determined set of energies of gamma rays following electron capture in $^{56}Co$ it is

TABLE I. Results of the elastic proton scattering experiments at the $E_p=1.75$ MeV resonance in $^{13}C(p,p)^{13}C$.

| | 1 $\mu g/cm^2$ target | | | 4 $\mu g/cm^2$ target | | |
|---|---|---|---|---|---|---|
| $J^\pi$ assumption | $\Gamma_p$ (eV) | $f/p$ ratio | $\chi^2/df$ | $\Gamma_p$ (eV) | $f/p$ ratio | $\chi^2/df$ |
| $2^+$ | $128\pm10$ | $-0.73\pm0.07$ | 1.61 | $125\pm14$ | $-0.73\pm0.11$ | 1.46 |
| $2^-$ | $55\pm9$ | | 6.98 | $63\pm13$ | | 4.74 |

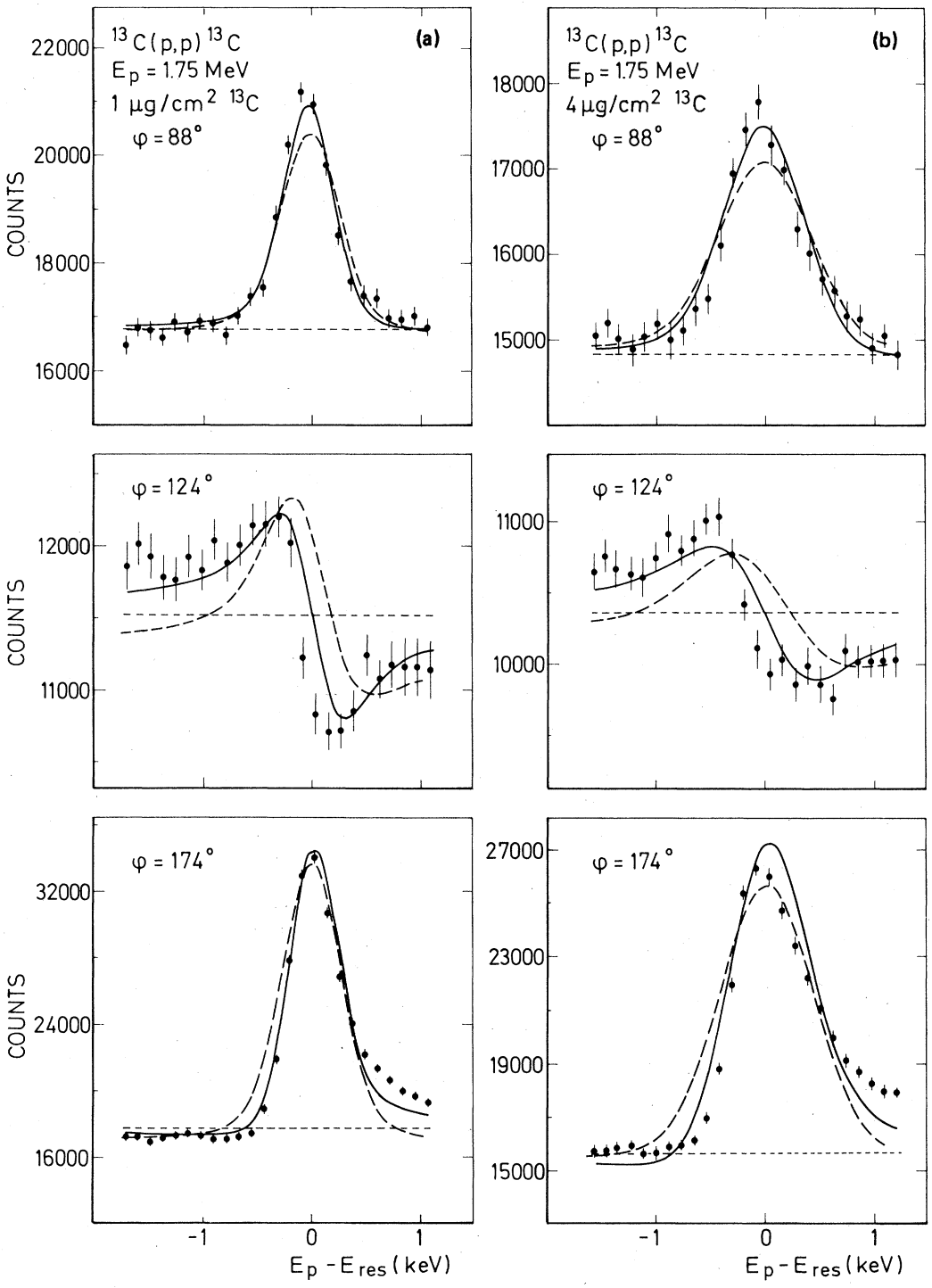


FIG. 2. Proton scattering yield curves as function of the effective proton energy at 1.75 MeV for (a) a 1 $\mu$g/cm$^2$ thick $^{13}$C target and (b) a 4 $\mu$g/cm$^2$ thick $^{13}$C target measured at three angles: 88°, 124°, and 174°. The solid line is the best fit with $J^\pi = 2^+$ to the data including a hard-sphere interference term. The dashed curve is the result of the best fit to the data after omitting the hard-sphere term. The dotted straight line indicates the potential scattering level.

possible in favorable cases to determine with a sub-keV precision the energy of gamma rays following a $(p,\gamma)$ reaction.[2] The $E_p = 1.75$ MeV resonance in $^{13}C(p,\gamma)^{14}N$ has a decay scheme convenient for this approach, as is illustrated in Fig. 3. Several cascades with components of energy less than 3.5 MeV (the highest accurately known energy in the $^{56}Co$ decay) are shown. Relevant portions of the spectrum (accumulated during 23 h) are shown in Fig. 4 (the dispersion is about 1 keV/channel). This spectrum was peak stabilized every minute with a precision pulser fed into the preamplifier. This produced a peak at the high energy end of the spectrum.

The misalignment of the beam spot with respect to the collimator axis was determined to be 0.11° $\pm$0.17° in the forward direction, which means that the energies found are slightly too high. The results are corrected for the influence of this misalignment, taking level lifetimes into account.

Following the procedure described in Ref. 2 the calibration lines were fitted with a Gaussian function and the resulting peak positions were fed into a computer code that produced the spectrum energy calibration in the form of a polynomial of the fifth degree. In total, 18 relations stemming from the $^{56}Co$ decay (13 transitions and five cascade/crossover relations) and five $^{14}N^*$ cascade/crossover relations (indicated as 1 to 5 in Fig. 3) were used, leading to a calibration fit with a normalized $\chi^2$ of 2.04. The results are presented in Table II, where the components of the cascades and the combined values are specified. Comparison with the values given in the Ajzenberg-Selove compilation[1] indicates a good agreement with the most accurate values given there and a discrepancy with the less precisely given energies of the 5.69, 5.83, and 6.45 MeV levels. As the 5.69 and 6.45 MeV levels show a cascade with individual transition energies less than 3.5 MeV, our values must be given more credibility than those cited in Ref. 1. The energy of the 7.03 MeV level is determined by subtracting the $(r \rightarrow 7.03)$ transition energy from the final value of the 9.17 MeV excitation energy. The same procedure was followed in the case of the 5.83 MeV level. The ground-state transition of the 5.83 MeV level was identified in the spectrum, but was omitted from the fit because extraction of an accurate peak position (value) was prevented by an underlying structure.

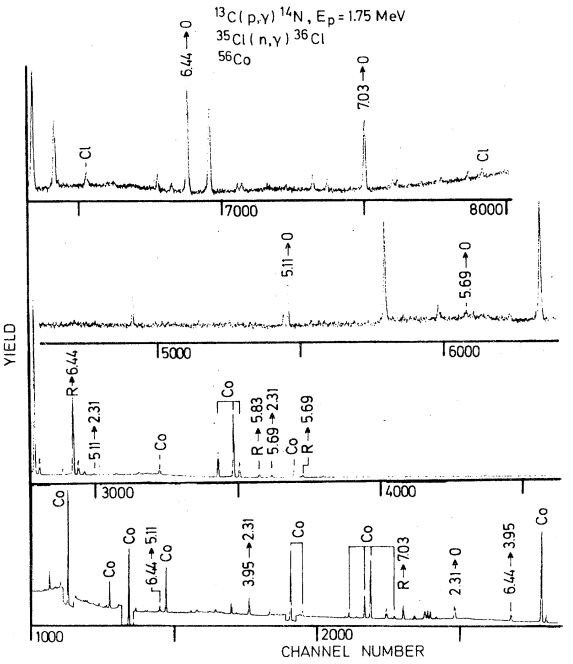


FIG. 4. Part of the spectrum obtained by simultaneous measurement of the decay of the 9.17 MeV level in $^{14}N$, the gamma rays from the $^{56}Co$ decay, and the lines produced by thermal neutron capture in $^{35}Cl$. The nature of most photopeaks is indicated. The dispersion is $\sim$1 keV/channel. Several regions are presented on a reduced scale.

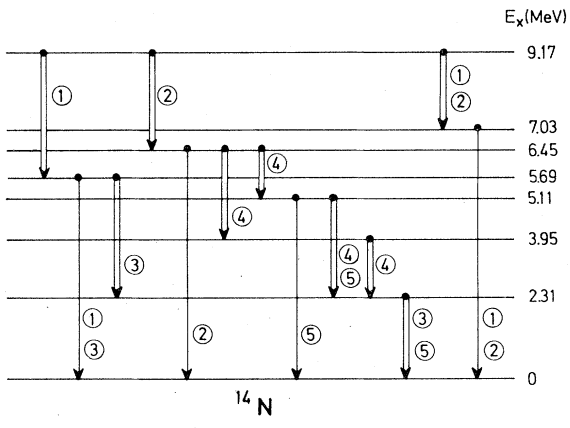


FIG. 3. Relevant part of the decay scheme of the 9.17 MeV resonance in $^{13}C(p,\gamma)^{14}N$. The transitions of energy less than 3.5 MeV are indicated with a double arrow. The cascade/crossover constraints used in the calibration fit are indicated as 1 to 5.

The final result for the excitation energy of the 9.17 MeV level is in good agreement with the value given in the $(p,\gamma)$ compilation (Table 14.20) of Ref. 1 and is slightly higher than (although not outside the error limits of) the energy given in Table 14.11

TABLE II. Results of the determination of excitation energies of levels in $^{14}$N and $^{36}$Cl and comparison with other work.

| $E_x$ in cascades[a] (keV) | Cascade sum (keV) | $E_x$ (keV) | $E_x$ in other work (keV) |
|---|---|---|---|
| | | 2312.90(3) | 2312.87(7)[d] |
| 1635.3(2) + 2312.90(3) | | 3948.2 (2) | 3947.8 (4)[d] |
| | 5105.6 (5)[b] | 5105.9 (3) | 5105.87(18)[d] |
| 2793.3(5) + 2312.90(3) | 5106.2 (5) | | |
| | 5692.1 (1.2)[b] | 5691.55(13) | 5689.6 (1.1)[d] |
| 3378.64(13) + 2312.90(3) | 5691.54(14) | | |
| | 6446.8 (1.2) | | |
| 2498.2(5) + 1635.3(2) + 2312.90(3) | 6446.4 (5) | 6446.3 (2) | 6444.4 (1.1)[d] |
| 1340.28(3) + 5105.9(3)[c] | 6446.2 (3) | | |
| 3481.2(5) + 5691.55(13)[c] | 9172.8 (5) | | |
| 2726.04(4) + 6446.3(2)[c] | 9172.4 (2) | 9172.5 (3) | 9170.8 (1.6)[d] |
| 2143.11(3) + 7029.7(1.2) | 9172.8 (1.2) | | 9172.5 (9)[e] |
| 9172.5(3) − 3338.14(10) | | 5834.3 (3) | 5832.4 (1.4)[d] |
| 9172.5(3) − 2143.11(3) | | 7029.4 (3) | 7027.9 (1.4)[d] |

[a]The notation 1635.2(2) means 1635.2 ± 0.2, etc. The uncertainties stated are based upon the statistical errors only (including correlation errors). The uncertainty introduced by a 2.6 ppm error in the Au calibration level has negligibly small influence on the results.

[b]Gamma-ray energies above 3.5 MeV were determined by extrapolation of the calibration curve, also using cascade/crossover relations in the decay of $^{14}$N*.

[c]In the calculation of the error, correlation effects due to multiple use of transitions were taken into account.

[d]Table 14.11 of Ref. 1.

[e]Table 14.20 of Ref. 1; the error is inferred from the uncertainty stated for $E_p$, and does not include the error in the $Q$ value of the $(p,\gamma)$ reaction.

of Ref. 1. As can be seen from Fig. 3 and Table II, the energy of the 9.17 MeV level is precisely determined by two cascades (via the 5.69 and 6.45 MeV levels) which have all components in the region covered by the $^{56}$Co decay lines.

## IV. RESONANCE ABSORPTION EXPERIMENTS

### A. Introduction

In nuclear photoexcitation studies several techniques have been employed.[8–12] A method which combines energy variability over a small range with high resolution and a photon flux of moderate intensity is the resonance gamma-ray absorption technique.[13,14] Several applications of the method have been made, mostly involving experiments where the emitting compound state and the absorber level are in nuclei of the same kind.[2,13–21] In some experiments it has been shown that this method can also be used to excite bound and unbound nuclear states with an appreciable ground-state transition in absorber nuclei of other elements.[22–24] Some limits of the method are discussed in a recent review article,[25] which also shows the availability of a matching gamma ray from a $(p,\gamma)$ reaction for practically any level within the energy range from 6 to 10 MeV.

### B. Experimental setup

The experimental setup is described in an earlier publication.[2] The target consisted of 50 $\mu$g/cm$^2$ $^{13}$C deposited on a 0.3 mm thick tantalum disc which formed part of the vacuum wall of the target holder. This chamber was connected with the beam pipe by means of a bellows which permitted the target to be rotated about its vertical axis over an angular range of $\pm 20°$. As the target holder was mechanically connected with (but electrically isolated from) the goniometer carrying the absorber, collimator, and detector, the angle between the plane of the target and collimator slit was constant during experiments. This angle was chosen

TABLE III. Characteristic data of the resonance absorption experiments with the $E_p = 1.75$ MeV resonance in $^{13}C(p,\gamma)^{14}N$ and a $lN_2$ absorber.

| | | | | | |
|---|---|---|---|---|---|
| absorber length (cm) | 64.0 | 32.0 | 16.0 | 8.0 | 4.0 |
| $n$ ($\times 10^{23}$ $^{14}N$ nuclei/cm$^2$) | 22.2 | 11.1 | 5.6 | 2.8 | 1.4 |
| number of runs over the angular range | 6 | 4 | 4 | 4 | 6 |
| measuring time (h) | 33 | 25 | 24 | 25 | 37 |

to be less than 35° so that the area of the beam spot projected perpendicularly to the collimator slit is considerably reduced in size.

The absorber was liquid nitrogen ($lN_2$) contained in a polystyrene reservoir of 32 cm internal length at 77 K. In a series of experiments the absorber length of $lN_2$ was varied from 32 to 4 cm by inserting hollow blocks of iron of suitable length. In the last experiment the 32 cm reservoir was replaced by a 64 cm container filled with $lN_2$. The resulting number of $^{14}N$ nuclei per cm$^2$ are given in Table III. In the reaction plane the collimator aperture amounted to 0.40° for the 32 cm reservoir and 0.34° for the 64 cm container, resulting in, respectively, about 270 and 230 eV instrumental width.

Figure 5 shows typical spectra of the resonance absorption detector, one in the dip center and one taken at a wing position. The window indicated by the vertical lines is used to extract the raw data, on which background corrections were performed. These amounted to less than 0.05%. The resulting transmission versus angle curves are shown in Fig. 6.

The goniometer was rotated about the target in 19 steps varying from 0.25° to 1.00° (corresponding to about 170 to 680 eV energy change). The smaller steps were taken near the center of the dip (80.8°). For each position the detector spectrum was stored for a fixed number of counts registered by a 7.5×7.5 cm NaI(Tl) monitor in a window covering the photopeak of the 9.17 MeV gamma ray. The entire experiment was computer controlled, with computerized peak stabilization of the NaI(Tl) detectors and computer positioning of the goniometer. In a separate experiment this positioning was found to be subject to a relative (random) error of 0.05°.

The measurements were split into a number of short runs of about 15 to 20 min duration at each angle. In Table I some relevant information is given. The whole experiment required about 144 h of running time, including a background measurement without the $lN_2$ absorber at a bombarding energy just below $E_p = 1.75$ MeV.

### C. The instrumental resolution function

The instrumental width is determined by the collimator slit and by the angular divergence of the protons. In our experiments this width is of the same order of magnitude as the level width under consideration, so direct observation is excluded. In

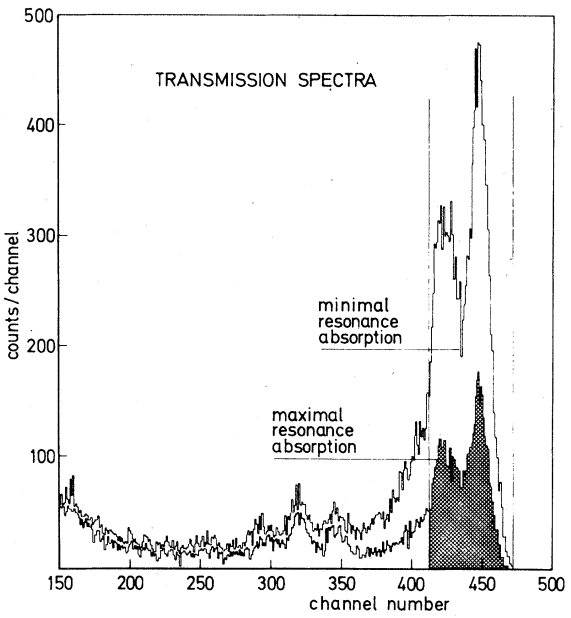


FIG. 5. Part of typical spectra obtained with the NaI(Tl) detector behind the collimator. The cross-hatched area represents the spectrum at resonance, where an appreciable amount of 9.17 MeV photons is removed from the beam. The other one is taken at a wing position with negligible resonance absorption. The absorber length is 64 cm $lN_2$. The vertical lines mark that part of the spectra used for extracating the raw data. Owing to the anticoincidence circuitry the double-escape peak has almost disappeared.

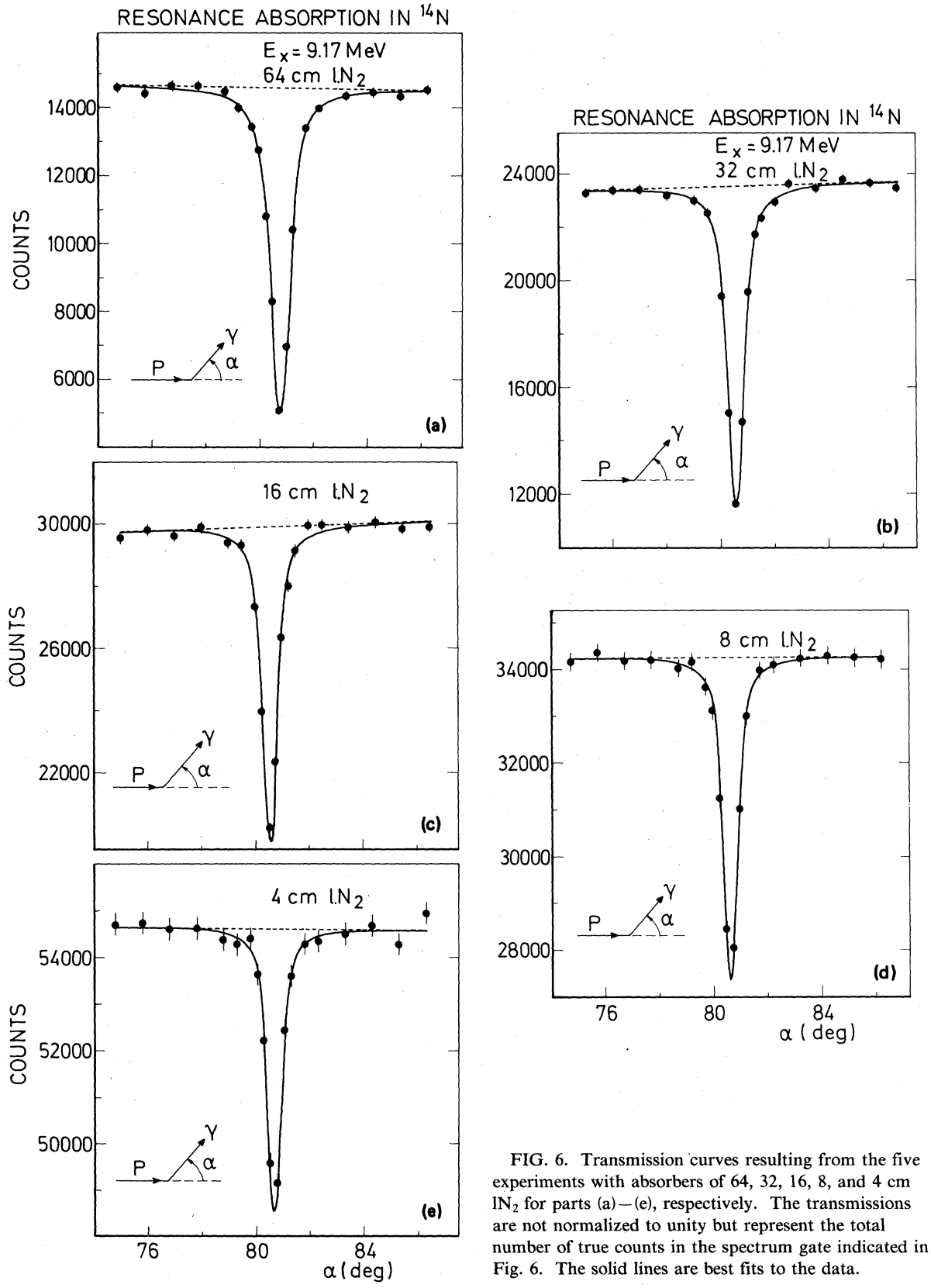


FIG. 6. Transmission curves resulting from the five experiments with absorbers of 64, 32, 16, 8, and 4 cm $lN_2$ for parts (a)—(e), respectively. The transmissions are not normalized to unity but represent the total number of true counts in the spectrum gate indicated in Fig. 6. The solid lines are best fits to the data.

order to establish the collimator transmission function a separate experiment was performed.

The experimental setup is shown in Fig. 7, together with measured and calculated curves. The agreement is quite satisfactory. Using this function the collimator transmission function was calculated (Fig. 8). All but 0.02% of the area is contained in a trapezium. As the angular spread of the protons is not well known, the overall instrumental resolution could not be predicted except in the sense that the dotted curve of Fig. 8 represents the limiting case of perfect collimation of the protons. As all resonance absorption experiments performed to date lend credence to the assumption of a Gaussian instrumental function, we have also plotted in Fig. 8 a Gaussian curve (the solid line) chosen such that the maximal function value is unity and the area under the curve equals the area under the trapezium.

### D. Transmission analysis

The general form of the transmission function $T(\alpha')$ is a double convolution:

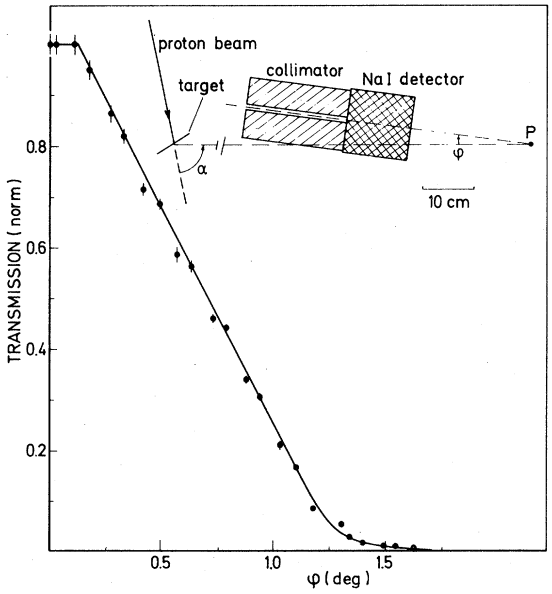


FIG. 7. Experimental and calculated results of the determination of the collimator transmission in the setup shown in the insert. The collimator-detector combination is rotated about an axis at $P$, and the transmission of the proton-induced gamma rays through the collimator is measured as a function of $\phi$. As this function is symmetric, only one-half of it is shown.

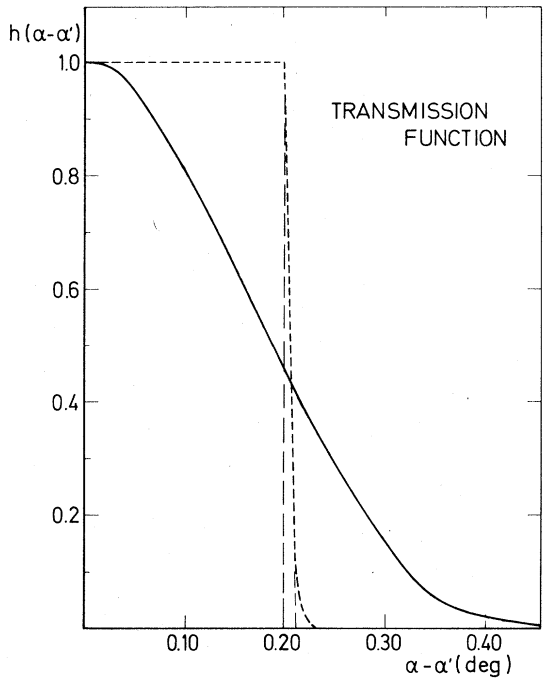


FIG. 8. Two approximations to the instrumental resolution function $h(\alpha-\alpha')$: the calculated collimator transmission function (where the dashed lines represent two possible approximations to the dotted curve—respectively, a rectangular block and a trapezium) and a Gaussian function (the solid line) chosen such that the enclosed area equals the area under the collimator transmission function. As $h$ is symmetric with respect to $\alpha-\alpha'=0$, only one-half of it is shown.

$$T(\alpha')=\frac{\int dE \int d\alpha\, h(\alpha-\alpha')g(E,\alpha)T(E)}{\int dE \int d\alpha\, h(\alpha-\alpha')g(E,\alpha)}, \quad (2)$$

where $h(\alpha-\alpha')$ represents the instrumental resolution function discussed in Sec. IV C, $g(E,\alpha)$ is the emitter function, and $T(E)$ is the transmission through the absorber. The emitter has the well-known Breit-Wigner shape, whereas the transmission is an exponential with a Breit-Wigner argument.

The data shown in Fig. 6 were analyzed with a computer code which performed a standard $\chi^2$ search for the optimal parameter set. The computations were based upon Eq. (2) and required numerical integration of that part of the double convolution not reducible to analytical forms. Two options in the fitting procedure (corresponding to the instrumental functions described in the preceding section) were applied, the results of which are given in Table IV. In the analysis the relative er-

TABLE IV. Results of the analysis of the resonance absorption experiments with the $E_p = 1.75$ MeV resonance in $^{13}C(p,\gamma)^{14}N$ and a $lN_2$ absorber for two options in the fitting procedure.

| Absorber length (cm) | Separate fits | | | | | Simultaneous fits | | | | |
|---|---|---|---|---|---|---|---|---|---|---|
| | $\Gamma$(eV) | $\Gamma_\gamma$ (eV) | $n\sigma_0$ | $A_\alpha$ (eV) | $\chi^2/df$ | $\Gamma$ (eV) | $\Gamma_{\gamma_0}$ (eV) | $n\sigma_0$ | $A_\alpha$ (eV) | $\chi^2/df$ |
| Gaussian instrumental function | | | | | | | | | | |
| 64 | 147±19 | 6.7±0.8 | 4.9±0.9 | 545±53 | 0.69 | | | 5.8 ±0.4 | 547±19 | |
| 32 | 133±15 | 7.5±0.6 | 3.0±0.4 | 370±33 | 0.72 | | | 2.9 ±0.2 | 363±14 | |
| 16 | 135±19 | 6.9±0.6 | 1.4±0.2 | 216±26 | 0.85 | 135±11[a] | 7.2±0.4[a] | 1.4 ±0.10 | 225±11 | 0.58 |
| 8 | 145±19 | 7.1±0.5 | 0.7±0.1 | 129±16 | 0.15 | | | 0.72±0.05 | 129± 7 | |
| 4 | 120±22 | 6.5±0.5 | 0.4±0.1 | 63 ±12 | 0.55 | | | 0.36±0.02 | 70 ± 4 | |
| trapezoidal instrumental function | | | | | | | | | | |
| 64 | 161±18 | 6.3±0.6 | 4.2±0.6 | 547±47 | 0.70 | | | 4.8 ±0.3 | 558±18 | |
| 32 | 148±16 | 7.1±0.6 | 2.6±0.3 | 370±32 | 0.74 | | | 2.4 ±0.2 | 365±15 | |
| 16 | 151±19 | 6.7±0.6 | 1.2±0.2 | 220±25 | 0.94 | 152±11 | 6.8±0.4 | 1.2 ±0.1 | 222±10 | 0.57 |
| 8 | 162±22 | 7.1±0.6 | 0.6±0.1 | 131±17 | 0.18 | | | 0.61±0.03 | 126± 7 | |
| 4 | 123±23 | 6.7±0.6 | 0.4±0.1 | 65±13 | 0.53 | | | 0.30±0.02 | 66 ± 3 | |

[a]Adopted as the best values from this analysis.

ror in the angle $\alpha'$ was transformed into a transmission error by use of a linearized approximation to the local shape of the transmission curve, and added in quadrature to the experimental transmission error. This has considerable influence in the dip region with its steep slopes.

The absorption integral[14] $A_\alpha$ was calculated from the results of the separate fits to the data. In Fig. 9 these values are displayed as a function of the absorber length $d$. From a simultaneous fit to the data the best parameter set is obtained and the curve of $A_\alpha$ vs $d$ using these parameter values in the theoretical expression[14] for $A_\alpha$ (including errors in the parameter values) is also indicated in the figure as the region between the solid lines. It can be concluded that both fit options give internally consistent results. This must be compared with Fig. 10, where the results of fitting the data with $\Gamma = 74$ eV (the mean value of other experiments[13,16]) are displayed. Here consistency is clearly lacking.

The procedures described by Hanna and Meyer-Schützmeister[13] were applied to the $A_\alpha$ values obtained from our measurements. The resulting values for $\Gamma$ are consistent with the results given in Table IV. We have also performed a reanalysis of their data with our computer code. If this is done with instrumental widths as specified by Hanna and Meyer-Schützmeister, a wide range of $\Gamma$ values (20–240 eV) is found from the different experiments. This is partly due to the fact that only a limited angular range was searched, resulting in a large uncertainty in the nonresonant transmission. Fits with $\Gamma = 135$ eV gave reasonable results.

In the publication of Luukko[16] the data were fitted with a Gaussian curve. To the absorption integral obtained in this way, a correction term (amounting to a maximum of about 40%) had to be added to account for the wing area beyond the region of measurement. As an even more limited angular range was scanned in Luukko's experiments, no precise value for $\Gamma$ could be obtained by our reanalysis. Fits with $\Gamma = 135$ eV also gave good results.

In the absence of knowledge regarding the exact shape of the instrumental resolution function (see Sec. IV C), the Gaussian approximation to $h(\alpha - \alpha')$ is regarded to be the best choice; the total level width as calculated from this analysis is therefore taken to be 135±11 eV (and $\Gamma_{\gamma_0}$ is taken to be 7.2±0.4 eV). The value for $\Gamma$ obtained in the analysis in which the trapezium was used for the instrumental function is larger than this, although not outside the combined error margins. The conclusion drawn from our resonance absorption experiments are in excellent agreement with the $(p,p)$ measurement.

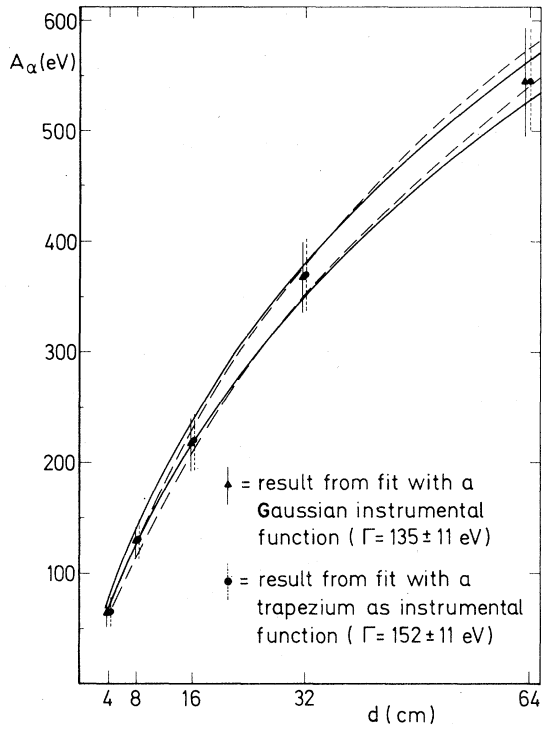


FIG. 9. The absorption integral $A_\alpha$ as a function of absorber length $d$. The data points represent values obtained from separate fits to the data. The dotted and solid lines mark bands of $A_\alpha$ values resulting from several simultaneous fits to the data, resulting in the best set of parameters for a given fit option. The solid lines arise from the fit option with a Gaussian instrumental function, while the dotted lines result from a fit with a trapezium for $h(\alpha-\alpha')$.

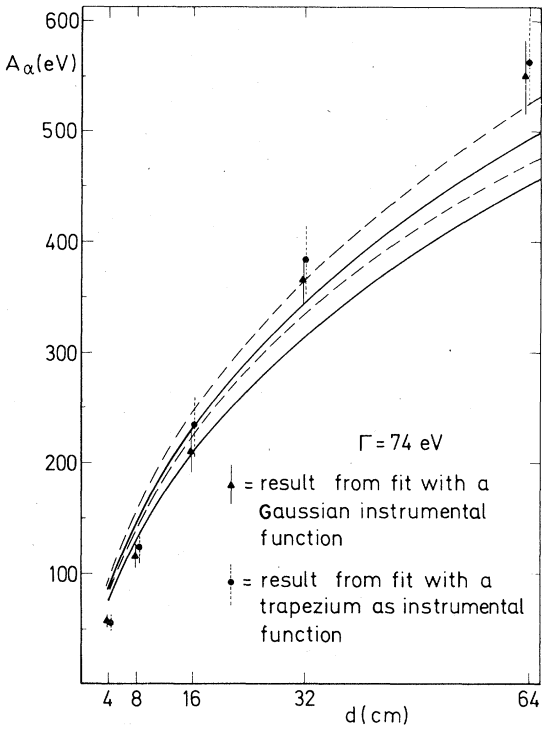


FIG. 10. The absorption integral $A_\alpha$ as a function of absorber length $d$. The data points represent values obtained from separate fits to the data with $\Gamma=74$ eV. The dotted and solid lines mark bands of possible $A_\alpha$ values resulting from several simultaneous fits to the data with $\Gamma=74$ eV. The solid lines arise from the fit option with a Gaussian instrumental function, while the dotted lines result from a fit with a trapezium for $h(\alpha-\alpha')$.

## V. RESONANCE FLUORESCENCE

### A. Introduction

The measurements described in this section were performed to prove the feasibility of resonance fluorescence measurements with gamma rays from $(p,\gamma)$ reactions, and to confirm the theoretically predicted azimuthal dependence of this scattering process. In other experiments performed in this laboratory[24] this technique has been used to determine the parity of electromagnetic transitions in $^{208}$Pb.

Experiments based on the same principle have been performed earlier with polarized photons arising from scattering of bremsstrahlung on a discrete level[26–28] and also, with considerable success, by making use of "tagged" polarized photons from bremsstrahlung.[29,30] The present method has the advantage of high resolution (several hundred eV) and of ease of background subtraction, since the resonance condition can be destroyed by rotating the goniometer just a few degrees. Nonresonant scattering processes are negligible for the combination of polar angle and the transition energy used.

### B. Theoretical background

We follow the standard convention[31] that for photons the polarization $\mathscr{P}$ is unity when the electric vector lies in the $\phi=0$ plane. The intensity distribution $W(\theta,\phi)$ (as measured by a polarization insensitive detector) of the scattering of photons of polarization $\mathscr{P}$, from a nucleus of ground-state spin $b$ and excited-state spin $a$, is

$$W(\theta,\phi)\simeq \sum_{L_1L_1'L_2L_2'k} \bar{Z}_1(L_2aL_2'a;bk)\bar{Z}_1(L_1aL_1'a;bk)Q_k\,[P_k(\cos\theta)+\mathscr{P}(-)^{\Pi_1'}\kappa_k(L_1L_1')P_k{}^2(\cos\theta)\cos2\phi] \times\langle a||L_1\,|\,b\rangle\langle a||L_1'\,|\,b\rangle^*\langle a\,|\,L_2||b\rangle\langle a\,|\,L_2'||b\rangle^* \,. \tag{3}$$

In this equation, $\Pi_1'$ (referring to the first, i.e., excitation, transition) is zero for electric multipoles and one for magnetic multipoles, and the $Q_k$ are the well-known angular distribution attenuation factors (assuming cylindrical detectors). The $\bar{Z}_1$ functions have been defined by Ferguson[32] and the $\kappa_k(LL')$ have been defined by Fagg and Hanna.[33]

In these measurements one determines the ratio $R$, defined as

$$R=\frac{W(\theta,0°)-W(\theta,90°)}{W(\theta,0°)+W(\theta,90°)}\,, \tag{4}$$

which for unmixed transitions (the case here) reduces to

$$R=\mathscr{P}(-)^{\Pi}\frac{\sum_k \kappa_k(LL)[\bar{Z}_1(LaLa;bk)]^2Q_kP_k{}^2(\cos\theta)}{\sum_k[\bar{Z}_1(LaLa;bk)]^2Q_kP_k(\cos\theta)}\times100\% \,. \tag{5}$$

In the particular case of a $1\to2\to1$ unmixed dipole transition for $\theta = 90°$

$$R=\mathscr{P}(-)^{\Pi}\frac{21Q_2}{80-7Q_2}\times100\% \,. \tag{6}$$

From the angular distribution measurements of Prosser *et al.*[3] it is known that the 9.17 MeV level in $^{14}$N decays by pure dipole radiation. In this case, at the polar angle $\alpha$, the polarization is given by[33]

$$\mathscr{P}=\frac{-\frac{1}{2}(-)^{\Pi}A_2P_2(\cos\alpha)}{1+A_2P_2(\cos\alpha)}\,. \tag{7}$$

With the measured[3] value of $A_2(-0.44\pm0.01)$ and the resonance angle of 80.8° we find for the resonance fluorescence experiment an expected value of

$$R_{\text{theor}}=-0.53\frac{21Q_2}{80-7Q_2}\times100\% \,. \tag{8}$$

Note that for this special case where the resonance fluorescence excites the same (pure) transition as that which produced the radiation, the experiment is *not* sensitive to the parity of the transition, but does permit verification of the correct functioning of the apparatus, and the interpretation.

### C. Experimental setup

The polarized 9.17 MeV photons from the $E_p=1.75$ MeV resonance in $^{13}$C$(p,\gamma)^{14}$N were scattered in a second target containing $^{14}$N. The setup is shown schematically in Fig. 11. The photons transmitted through the collimator are almost monoenergetic and the azimuthal distribution of resonantly scattered photons is measured by two detectors at $\phi=0°$ and 90°, respectively. The background can be obtained by rotating the goniometer with the collimator, scatterer, and detector over a few degrees, enough to destroy the energy matching condition.

With this technique a high resolution can be reached, which implies the necessity of an exact determination of the resonance angle in Fig. 11.

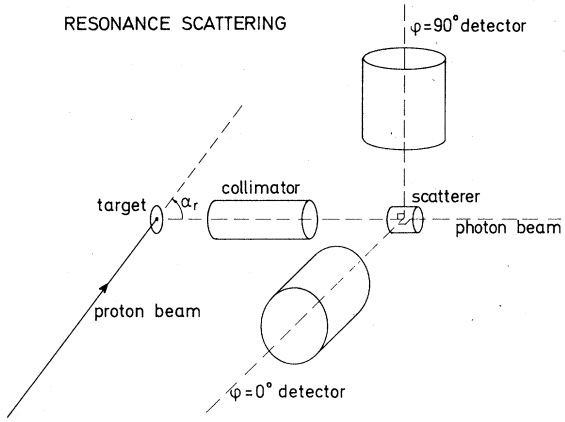


FIG. 11. Schematic drawing of the setup used for the resonance scattering of plane-polarized photons. In the azimuthal plane the angular distribution of the scattered photons is measured with the two detectors indicated. The active and passive shielding has been omitted for clarity.

This was found in the resonance absorption measurements described in the preceding section. As the counting rates in the azimuthal plane are low, it is necessary to minimize the scatter-detector distance. On the other hand, polarization information is diminished with increasing solid angle subtended by the scatterer-detector combination due to smaller attenuation coefficients. These and other considerations led to an experimental configuration depicted in Fig. 12. Heavy shielding of the detectors against direct transmission from the target is necessary to keep the background low, and to reduce the counting rate in the anticoincidence shield. The scatterer is a 5.2 cm long BN cyclinder of 3.9 cm diameter. The detectors are $7.5\times7.5$ cm NaI(Tl) crystals. The active shielding consists of a $22.5\times30$ cm NaI(Tl) ring crystal and a $30\times40$ cm plastic scintillator. The NaI(Tl) crystal was kindly lent to us by the R. J. van de Graaff Laboratory of the University of Utrecht and the plastic scintillator by the Zeeman Laboratory of the University of Amsterdam. The spectra were peak stabilized with an $^{88}Y$ source placed next to the scatterer.

During the experiment the goniometer was rotated to positions on and off resonance as well as to two positions in the flanks of the resonance. This is illustrated in Fig. 13, where the results of the measurements are shown together with the resonance absorption dip as found with the $7.5\times12.5$ cm NaI(Tl) detector behind the scatterer. The scattering spectra corresponding to the data points in Fig. 13 are shown in Fig. 14. As a check on instrumental effects the experiment was repeated with the $7.5\times7.5$ cm NaI(Tl) detectors plus electronics interchanged. Within the experimental error no difference could be noted.

The whole experiment was computer controlled, and was subdivided in short runs of about 10 min duration at each angle. For each position the detector spectra were stored for a fixed number of counts registered by a $10\times10$ cm NaI(Tl) monitor in a window covering the photopeak and both es-

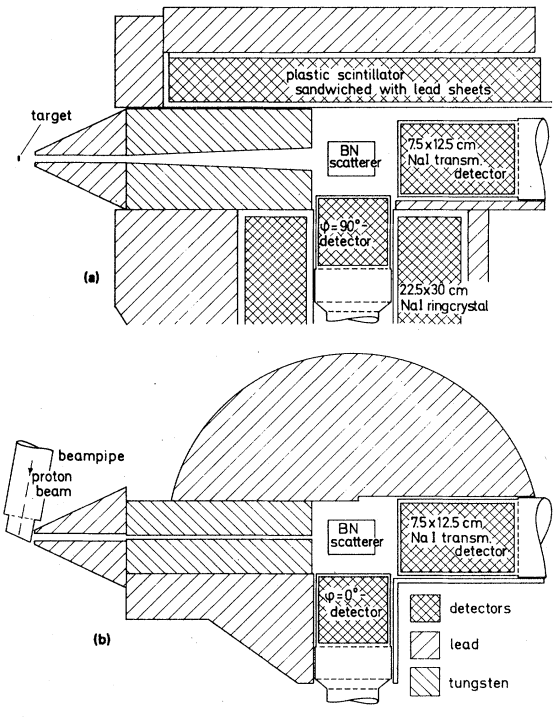


FIG. 12. Experimental configuration used to measure the azimuthal distribution of the elastic scattering of monoenergetic plane-polarized photons (a) in elevation, and (b) in plan view.

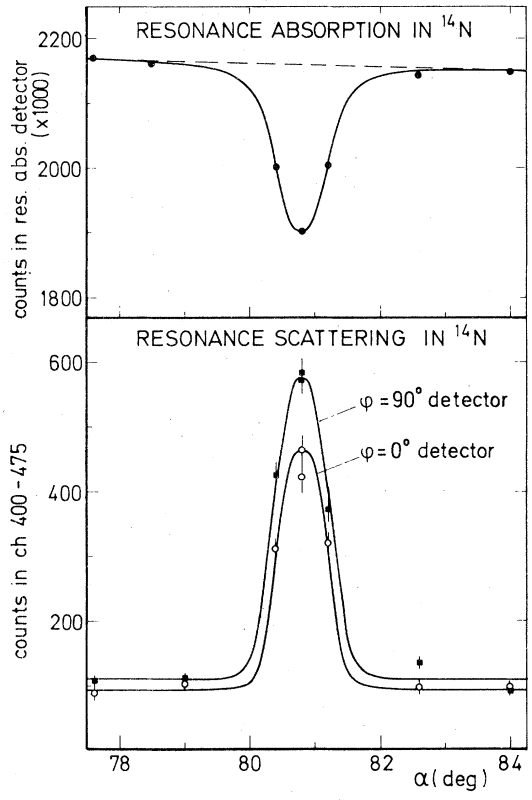


FIG. 13. Results of the scattering experiments. The upper part of the figure shows the transmission as function of angle $\alpha$, measured by a detector behind the scatterer and indicating the exact gamma ray matching conditions at 80.8° In the lower part the corresponding data points from both detectors in the azimuthal plane are depicted with error bars. The solid lines are not the result of fits to the data, but are merely a guide to the eye.

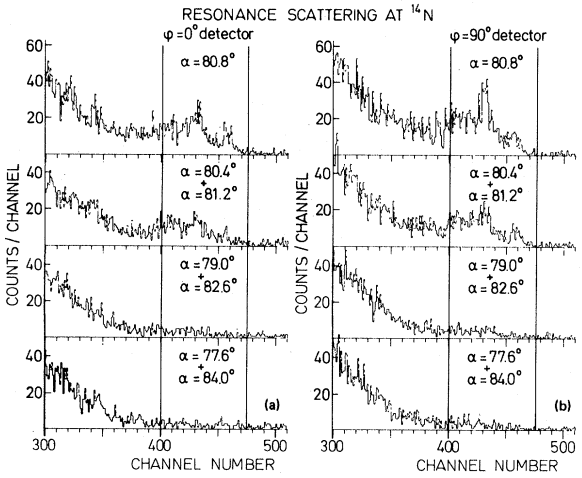


FIG. 14. Parts of the spectra of the NaI(Tl) detectors in the azimuthal plane as function of angle $\alpha$. The solid vertical lines mark the area used for obtaining the final values of $R_{exp}$.

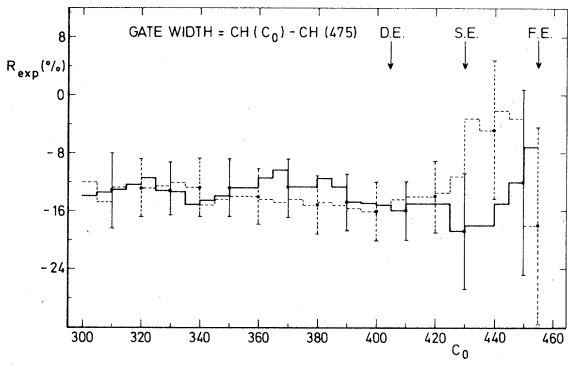


FIG. 15. Histogram of $R_{exp}$ as function of the gate width set on the spectra shown in Fig. 15. The first channel is $C_0$, and the last gate channel is channel 475. The solid line with associated error bars results from the first measurement. The dotted line stems from the observation after interchanging the detectors in the azimuthal plane.

cape lines of the 9.17 MeV gamma ray. This monitor was placed at a distance of 1 m from the target. The angular range was covered many times: 30 series in the first experiment and after interchanging the detectors another 22 series, requiring a total running time of 67 h. With a proton beam of 50 $\mu$A a signal-to-background ratio of about 6 was achieved. A typical background counting rate in the relevant part of the spectrum is 0.11 counts/min. Neutron production in the target did not pose serious problems in these experiments because of the rather low bombarding energy and the relatively high gamma-ray energy.

### D. Results

The measured ratio $R_{exp}$ from the experiments described above was $-15\pm3\%$. In Fig. 15 this ratio is plotted as function of the gate width set on the spectra. Within the statistical accuracy obtained, $R_{exp}$ is constant over a wide range of gates from below the double escape peak to the photopeak, indicating an internally consistent result. If 0.72 is used for the finite angle attenuation coefficients $Q_2$ we would expect from Eq. (8) a value of $-11\%$. An attenuation of $Q_2=0.72$ is the lowest possible value, corresponding to the "any interaction" assumption. Our geometry is not properly cylindrical (see Fig. 12) but the deviation from cylindrical symmetry is not enough to seriously affect the result. Using a value of $Q_2=1$, one would expect $R=-15\%$. The agreement is satisfying and can be considered as a quantitative proof of the methods used.

## VI. SUMMARY AND DISCUSSION

In the preceding sections several experimental techniques have been discussed in order to obtain accurate and reliable values for the parameters of the 9.17 MeV level in $^{14}$N. The results are summarized and compared with those given by the compilation of Ajzenberg-Selove[1] in Table V. The agreement between our $\Gamma$ values obtained by elastic proton scattering and resonance absorption is convincing. The discrepancy with the stated literature values from resonance absorption experiments can be explained as resulting from differences in methods of analysis (Sec. IV D). The literature value from a $(p,\gamma)$ study[34] is also given, for completeness, in Table V. This value has a large error margin as it was obtained by inspection of the yield curves. Our determination of $\Gamma_{\gamma_0}$ is in agreement with the value of $6.1\pm0.8$ eV given in Table V, which is the product of multiplication of the ground-state branching ratio and the $\Gamma_\gamma$ value quoted from Table 14.12 of Ref. 1.

The excitation energy of the 9.17 MeV level has been obtained with sub-keV accuracy with a cascade/crossover method. In this process the energies of five other $^{14}$N levels have been determined

TABLE V. Comparison of the results of this work with the Ajzenberg-Selove compilation (Ref. 1).

| | This work | | | |
|---|---|---|---|---|
| | $(p,p)^a$ | $(\gamma,\gamma)^b$ | cascade/crossover | Ref. 1 |
| $E_p$ (keV) | | | | 1746.6± 0.9[d] |
| $E_x$ (keV) | | | 9172.5±0.3 | 9172.5± 0.9[d] |
| | | | | 9170.8± 1.6[e] |
| $\Gamma_{\gamma_0}/\Gamma_\gamma$ (%) | | | | 79 ± 4 |
| $\Gamma$ (eV) | 135±8 | 135 ±11 | | 74 ± 8[e] |
| | | | | 70 ±50[f] |
| $\Gamma_{\gamma_0}$ (eV) | | 7.2±0.4 | | 6.1± 0.8[g] |
| $J^\pi$ | $2^+$ | | | $2^+$ [d,e,h] |

[a]The $^{13}C(p,p)$ studies in Sec. II.
[b]The resonance absorption experiments described in Sec. IV.
[c]The cascade/crossover method described in Sec. III.
[d]Cited from Table 14.20 of Ref. 1. The error is inferred from the uncertainty stated for $E_p$, and does not include the error in the $Q$ value of the $(p,\gamma)$ reaction.
[e]Cited from Table 14.11 of Ref. 1.
[f]Cited from Table 14.20 of Ref. 1, and based upon $(p,\gamma)$ measurements only.
[g]Product of multiplication of $\Gamma_{\gamma_0}/\Gamma = 0.79\pm0.04$ eV and $\Gamma_\gamma = 7.7\pm0.9$ eV as quoted in Ref. 1.
[h]Cited from Table 14.12 of Ref. 1.

with better precision than previous literature values. The $J^\pi$ assignment to the 9.17 MeV level has been placed on a solid basis by means of the elastic proton scattering experiment described.

In the last section a nuclear resonance fluorescence experiment was described involving the measurement of the azimuthal distribution of the elastic scattering of monoenergetic partially plane-polarized 9.17 MeV photons at the 9.17 MeV level in $^{14}N$. The qualitative and quantitative agreement between experiment and calculation is satisfying. As this method utilizes only the well-established theory of electromagnetic transitions, it is in essence model independent. In view of the many conflicting $J^\pi$ assignments (based upon different techniques), this method can be useful in the case of investigation of the electric or magnetic nature of the dipole transitions in such heavy nuclei as $^{208}Pb$.[24]

The authors wish to acknowledge the help of J. L. W. Petersen in the fabrication of the Si detectors, of J. L. Stavast, S. Brandenburg, and S. van der Hoek, and of our other colleagues in the Van de Graaff accelerator group for assistance during the measurements and discussion of the results.

[1]F. Ajzenberg-Selove, Nucl. Phys. A268, 1 (1976).
[2]W. Biesiot, Ph.B. Smith, J. L. Stavast, P. B. Goldhoorn, and S. van der Hoek, Nucl. Phys. A359, 149 (1981).
[3]F. W. Prosser, Jr., R. W. Krone, and J. J. Singh, Phys. Rev. 129, 1716 (1963).
[4]H. J. Rose, W. Trost, and F. Riess, Nucl. Phys. 12, 510 (1959).
[5]H. J. Rose, Nucl. Phys. 19, 113 (1960).
[6]R. Huby, Proc. Phys. Soc. (London) 67, 1103 (1954).
[7]A. A. Strassenburg, R. E. Hubert, R. W. Krone, and F. W. Prosser, Bull. Am. Phys. Soc. 3, 372 (1958).
[8]F. R. Metzger, Progr. Nucl. Phys. 7, 54 (1959).
[9]B. Arad and G. Ben-David, Rev. Mod. Phys. 45, 230 (1973).
[10]C. Schuhl, in Proceedings of the International Conference on Photonuclear Reactions and Applications, edited by B. R. Berman (LLL, Livermore, California, 1973), p. 1249.
[11]S. J. Skorka, in *The Electromagnetic Interaction in*

*Nuclear Spectroscopy,* edited by W. D. Hamilton (North-Holland, Amsterdam, 1975).
[12]R. Bergère, in *Photonuclear Reactions I,* edited by S. Costa and C. Schaerf (Springer, Berlin, 1977).
[13]S. S. Hanna and L. Meyer-Schützmeister, Phys. Rev. 108, 1644 (1957); 115, 986 (1959).
[14]P. B. Smith and P. M. Endt, Phys. Rev. 110, 397 (1958); 110, 1442 (1958).
[15]W. L. Mouton and P. B. Smith, Nucl. Phys. 16, 206 (1960).
[16]A. Luukko, Commun. Math Phys. 31, 1 (1965).
[17]C. van der Leun and N. C. Burhoven Jaspers, Nucl. Phys. 88, 235 (1966).
[18]P. R. de Kock, J. W. Koen, and W. L. Mouton, Ann. Phys. (N. Y.) 47, 481 (1968).
[19]J. W. Maas, Ph.D. thesis, Utrecht, 1976 (unpublished).
[20]R. J. Sparks, Nucl. Phys. A265, 429 (1976).
[21]H. van Rinsvelt and P. B. Smith, Physica (Utrecht) 30, 59 (1964).
[22]P. B. Smith, Phys. Rev. C 13, 2071 (1976).
[23]R. Sparks, H. Lancman, and C. van der Leun, Nucl. Phys. A259, 13 (1976).
[24]W. Biesiot and P. B. Smith, Phys. Rev. C 24, 808 (1981).
[25]A. P. M. van 't Westende, H. Lancman, and C. van der Leun, Nucl. Instrum. Methods 151, 205 (1978).
[26]H. Arenhövel and E. Hayward, Phys. Rev. 165, 1170 (1968).
[27]E. Hayward, W. C. Barber, and J. Sazama, Phys. Rev. C 8, 1065 (1973).
[28]E. Hayward, W. C. Barber, and J. J. McCarthy, Phys. Rev. C 10, 2652 (1974).
[29]M. M. May, Phys. Rev. 84, 265 (1951).
[30]A. M. Nathan, R. Starr, R. M. Laszewski, and P. Axel, Phys. Rev. Lett. 42, 221 (1979).
[31]U. Fano, J. Opt. Soc. Am. 39, 859 (1949).
[32]A. J. Ferguson, *Angular Correlation in Gamma-Ray Spectroscopy* (North-Holland, Amsterdam, 1965).
[33]L. W. Fagg and S. S. Hanna, Rev. Mod. Phys. 31, 711 (1959).
[34]R. O. Bondelid and C. A. Kennedy, Phys. Rev. 115, 1601 (1959).